DOI: 10.1080/01468030.2011.652803

Fiber and Integrated Optics, 31:186–195, 2012

ISSN: 0146-8030 print/1096-4681 online
DOI: 10.1080/01468030.2011.652803

Taylor & Francis
Taylor & Francis Group

Efficient Technique to Control the Zero-Dispersion Wavelength of a Microstructured Optical Fiber

RODDY E. RAMOS-GONZÁLES,[1,2]
ENVER FERNANDEZ-CHILLCCE,[2] LUIZ C. BARBOSA,[2]
and HUGO E. HERNÁNDEZ-FIGUEROA[1]

[1]Department of Microwaves and Optics, School of Electrical and Computer Engineering, University of Campinas, Sao Paulo, Brazil
[2]Department of Quantum Electronics, Gleb Wataghin Physics Institute, University of Campinas, Sao Paulo, Brazil

Abstract *An efficient technique to control the zero-dispersion wavelength of a microstructured optical fiber is proposed and numerically demonstrated in this article. This technique is based on the variation of the linear refractive index and the thickness of a thin film covering the microstructured optical fiber holes' inner surfaces. A powerful and accurate code based on a full-vector finite-element method formulation in conjunction with perfectly matched layers was used. A maximum of 570-nm zero-dispersion wavelength displacement is demonstrated. This thin film can be included after the microstructured optical fiber has been fabricated, as that means the zero dispersion of such fiber can be tailored as needed.*

Keywords finite-element method, microstructured optical fibers, thin film devices, zero dispersion

1. Introduction

A microstructured optical fiber (MOF) is a kind of photonic crystal fiber (PCF) that consists of a clad region with a periodic microstructure, resulting in a fiber with very different properties from conventional fibers. PCFs can guide light in two different ways. The solid-core PCFs guide light by the total internal reflection mechanism. On the other hand, the hollow-core PCFs guide light by the band gap effect. Lately, PCFs have attracted a great deal of interest because of their unusual and powerful properties [1–3], the most important being its chromatic dispersion control because of its application into optical fiber communication and non-linear optics. It has been reported that PCFs can realize flexible chromatic dispersion over a wide wavelength range [4–6]. The zero-dispersion wavelength (ZDW) of PCFs is one of the most important parameters to be considered in the fabrication of optical devices used in optical communication [7]. Various numerical methods can be used to design and model PCFs [7]. However, in order to model PCFs

Received 3 August 2011; accepted 20 December 2011.
Address correspondence to Mr. Roddy E. Ramos-Gonzáles, Department of Microwaves and Optics, School of Electrical and Computer Engineering, University of Campinas, DMO-FEEC-UNICAMP, Campinas, Sao Paulo, CEP 13083-970, Brazil. E-mail: roddyramos@gmail.com

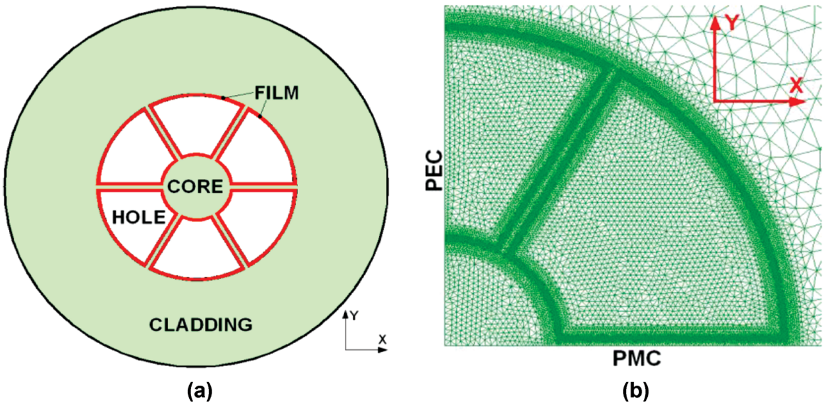

Figure 1. (a) Schematic illustration of the proposed MOF structure transverse cross-section of MOFs and (b) finite-element mesh—one-fourth of the transverse section of the fiber used in the analysis. (color figure available online)

accurately, it is crucial to use a powerful and efficient numerical method, such as the nodal finite-element method (FEM) full-vector model adopted here as simulation tool [8–10].

This work proposes an original technique for controlling the ZDW of an MOF by using a thin film covering the inner surfaces of the MOF holes; see Figure 1. This film may be placed in the holes in two ways. First, the fiber may be fabricated using two materials of similar mechanical properties but different refractive indexes. Second, after the fiber fabrication, the fiber holes may be covered with a thin film.

2. Analysis and Method

The FEM code used in this study discretizes the double-curl Helmholtz-type equation [8] in terms of the magnetic field H. The solution of the resultant matrix eigenvalue equation produces eigenvectors and eigenvalues, which contain the discrete magnetic field values and $-\beta^2$, respectively. Here, β represents the modal propagation constant. The real and imaginary parts of the effective index n_{eff} of the guided mode are next obtained by $n_{eff} = \beta/k_0$, where k_0 is the free-space wavenumber.

The MOF chromatic dispersion is calculated from the real part of the effective index n_{eff} according to the following expression [4, 10]: $D = -(\lambda/c)(d^2\,\mathrm{Re}[n_{eff}(\lambda)]/d\lambda^2)$, where λ is the wavelength, c is the velocity of light in a vacuum, and Re stands for the real part.

Figure 1a shows the MOF cross-section image, where x and y are the transverse directions, and z is the propagation direction. This silica MOF has six air holes around the solid core. A thin film covers the inner surface of the holes. The characteristics (thickness and linear refractive index) of the film are shown in Table 1.

In order to reduce the number of unknowns, the MOF symmetry can be exploited, and only one-fourth of the whole domain must be taken into account [4, 7–13]. Perfectly electric conductor (PEC) and perfectly magnetic conductor (PMC) boundaries ought to be considered here.

Figure 1b shows a mesh used to obtain the results presented in this work. The mesh is refined in the region around the film. The mesh was used to simulate the MOF with film thicknesses ranging from 50 nm to 500 nm.

Table 1
MOF and thin film parameters

Symbol	Quantity	Values
Nc	Film refractive index	1.32 to 3.50
FT	Film thickness	50, 100, 200, 500 nm
	Fiber core diameter	10 μm
	Structure diameter	30 μm
	Silica bridges thickness	0.5 μm

The mesh is composed of triangular elements (approximately 70,000), and the anisotropic perfectly matched layers (PMLs) were incorporated as absorbing boundary conditions [9, 10]. It is known that the fundamental HE_{11} mode is degenerated (HE_{11}^X and HE_{11}^Y). Thus, for the PMC (x-axis) and the PEC (y-axis), only the fundamental HE_{11}^Y mode was analyzed. It is assumed that the wave propagates in the z-direction [8].

In the calculations, the film refractive index was considered independent of the wavelength (from 1.0 μm to 1.8 μm). On the other hand, the silica material dispersion (given by Sellmeier's formula) was included [14].

3. Results and Discussion

The effective index is obtained for each operating wavelength and for different film parameters (Nc and FT).

Figure 2 shows the effective indexes of the fundamental mode HE_{11}^Y versus the wavelength for different Nc values. In both Figures 2a and 2b, some curves are truncated because only situations where the core power of the fundamental mode was greater or equal to 80% were taken into account. For shorter wavelengths ($\lambda \leq 1.41$ μm for $Nc = 3.00$ and $FT = 50$ nm, $\lambda \leq 1.19$ μm for $Nc = 2.75$ and $FT = 50$ nm, $\lambda \leq 1.21$ μm for $Nc = 1.52$ and $FT = 500$ nm, $\lambda \leq 1.35$ μm for $Nc = 1.53$ and $FT = 500$ nm), the power in the core drops rapidly (see Figures 3a and 3b). Figure 2a

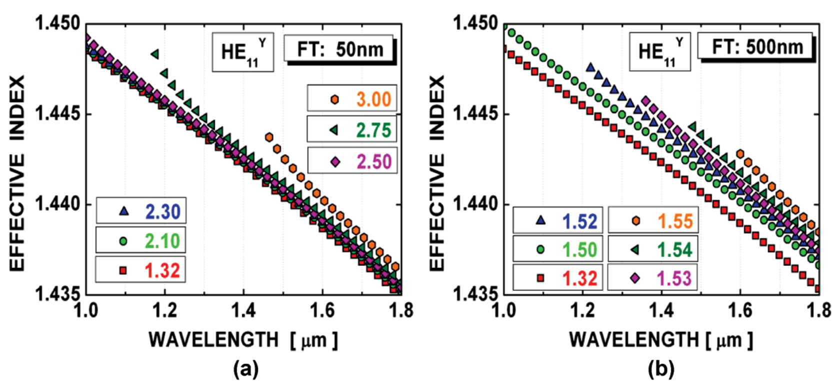

Figure 2. Effective refractive index of the fundamental mode HE_{11}^Y as a function of the wavelength for film thickness of: (a) 50 nm and (b) 500 nm. Only situations where the core power ≥80% were taken into account. (color figure available online)

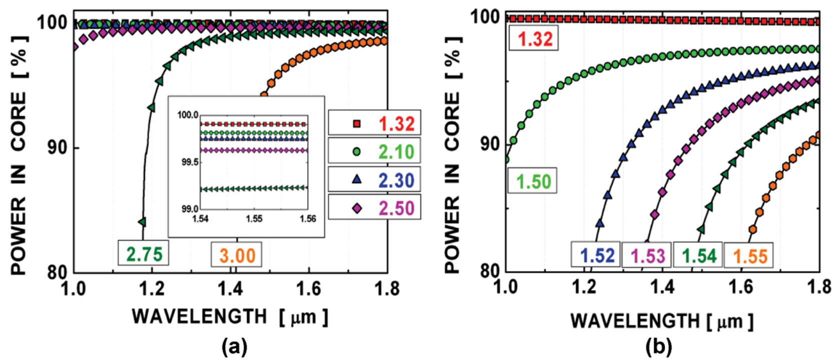

Figure 3. Power in the MOF core of the fundamental mode HE_{11}^{Y} as a function of the wavelength and different values of Nc for film thicknesses of: (a) 50 nm and (b) 500 nm. (color figure available online)

shows the behavior of the effective indexes for diverse refractive indexes of the film ranging from 1.32 to 3.00 when the film thickness is 50 nm. Figure 2b shows the behavior of the effective indexes for diverse refractive indexes of the film ranging from 1.32 to 1.55 when the film thickness is 500 nm.

In both figures, it was observed that the effective index decreases when the wavelength increases. For both film thicknesses, it was also observed that the effective index increases when the refractive index of the film increases. This behavior is the same as that of film thicknesses (100 nm and 200 nm) analyzed here.

Figure 3 shows the power of the HE_{11}^{Y} mode in the MOF core (core power/total power [%]). It is possible to observe that the power of the HE_{11}^{Y} mode is confined to the MOF core (over 80%) for modes whose effective indexes are shown in Figure 2. Figure 3a shows the behavior of the power of the fundamental mode for diverse refractive indexes of the film ranging from 1.32 to 3.00 when the film thickness is 50 nm. It is possible to observe that the power of the modes is over 98% when Nc varies from 1.32 to 2.50 for wavelengths ranging from 1.0 μm to 1.8 μm. When $Nc = 3.00$, the mode is located only at the MOF core for wavelengths >1.4 μm. Figure 3b shows the behavior of the power of the fundamental mode for diverse refractive indexes of the film ranging from 1.32 to 1.55 when the film thickness is 500 nm. This figure shows that the power of the modes is over 90% when Nc varies from 1.32 to 1.50 for the same wavelength ranges. When $Nc = 1.55$, the mode is in the MOF core for wavelengths >1.6 μm.

This demonstrates that the thickness and the refractive index of the film affect the power of the mode. For a thick film, the mode confinement is affected by a smaller variation of Nc than for a thin film.

Figures 4 and 5 show the normalized power profile of the Poynting vector module $|Sz|$ of the principal mode, where the intensity contours are uniformly spaced.

Figures 4a and 4b show the almost circular power field profile at the fiber core, considering a thickness of 50 nm and $Nc = 1.32$ and 2.50. In these figures, the film does not influence the profile. Figure 4c shows a "distorted" power profile, which is still located near the film (for $Nc = 3.00$). For these first three cases, the fundamental mode is the mode HE_{11}^{Y} ($FT = 50$ nm, $\lambda = 1.55$ μm, and $Nc \leq 3.00$). For $Nc = 3.50$ and over, the power profile is located in the film (Figure 4d). In this case, this is a surface mode that appears for specific film refractive indexes ($Nc > 3.00$).

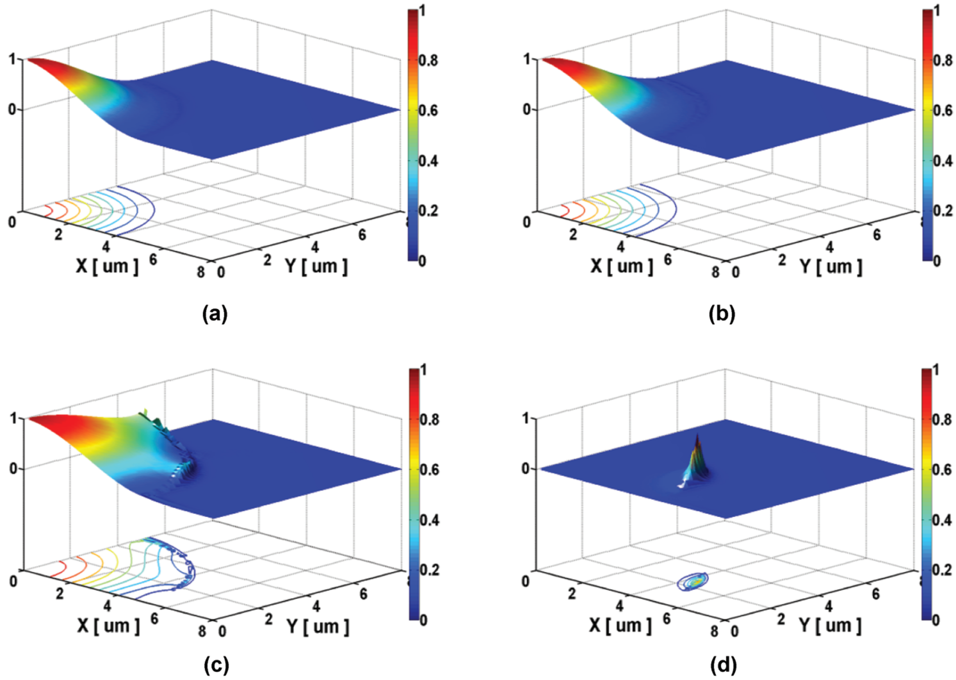

Figure 4. Power profile related to the principal mode Poynting vector module $|Sz|$. In this case, the film thickness is 50 nm, the wavelength propagation is $\lambda = 1.55$ μm, and four values of the film index were considered: (a) $Nc = 1.32$, (b) $Nc = 2.50$, (c) $Nc = 3.00$, and (d) $Nc = 3.50$. (color figure available online)

Figures 5a and 5b show the power field profile located in a film of 100 nm, considering the film index of 2.00 and wavelengths at 0.4 μm and at 0.8 μm. In these cases, this is a surface mode that appears for specific wavelengths ($\lambda < 1.2$ μm). For $\lambda = 1.2$ μm (Figure 5c), the power profile covers the core, film, and bridges. For $\lambda = 1.8$ μm, the power profile is circular (Figure 5d), and it is well confined to the MOF core. For the latter two cases, the fundamental mode is the mode HE_{11}^{Y} ($FT = 100$ nm, $Nc = 2.00$, and $\lambda \geq 1.2$ μm).

To calculate the chromatic dispersion, the effective indexes shown in Figure 2 have been considered.

Figure 6 shows the dispersion behaviors for different film thicknesses (50 nm to 500 nm) and Nc values (1.32 to 3.00). All these figures show ZDW displacement behaviors shifting to the infrared region when Nc increases.

From Figures 6a to 6d, it can be observed that different combinations of FT and Nc provide wide ZDW displacements, taking as reference the MOF without a film whose ZDW occurs at $\lambda_{ZDW0} = 1.15$ μm, and its location is pointed out in all dispersion plots through a vertical dotted line. For the same ZDW displacement, the thicker FT is, the smaller Nc is. For instance, to obtain a displacement of 570 nm, FT and Nc are 50 nm and 3.00, respectively; see Figure 6a. For almost the same displacement, 560 nm, on the other hand, FT and Nc are 500 nm and 1.54, respectively; see Figure 6d. Table 2 lists the widest ZDW displacements obtained with the variation of FT and Nc shown in Figure 6.

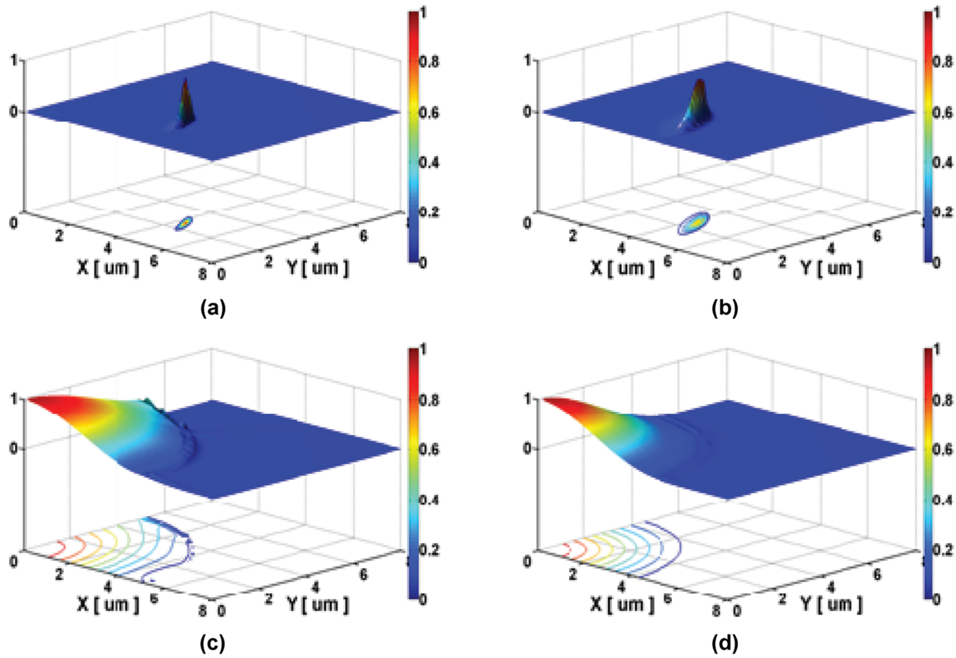

Figure 5. Power profile related to the principal mode Poynting vector module $|Sz|$. In this case, the film thickness is 100 nm, the film index is 2.00, and four values of the wavelength were considered: (a) $\lambda = 0.4$ μm, (b) $\lambda = 0.8$ μm, (c) $\lambda = 1.2$ μm, and (d) $\lambda = 1.8$ μm. (color figure available online)

Figure 7 shows the displacements obtained by fixing Nc and varying FT. Figure 7a shows the dispersion for $Nc = 2.00$ and $FT = 50$ and 100 nm. The ZDW displacement obtained with $FT = 50$ nm and 100 nm were of 10 nm and 220 nm, respectively. Figure 7b shows the dispersion for $Nc = 2.10$ and $FT = 50$ nm, 75 nm, and 100 nm. Here, the ZDW displacement obtained with $FT = 50$ nm, 75 nm, and 100 nm were of 10 nm, 80 nm, and 420 nm, respectively.

Table 2
Widest ZDW displacements taking as reference $\lambda_{ZDW0} = 1.15$ μm

FT (nm)	Nc	ZDW displacement (nm)
50	3.00	~570
	2.75	~290
100	2.10	~420
	2.00	~220
200	1.75	~440
	1.70	~250
500	1.54	~560
	1.53	~440

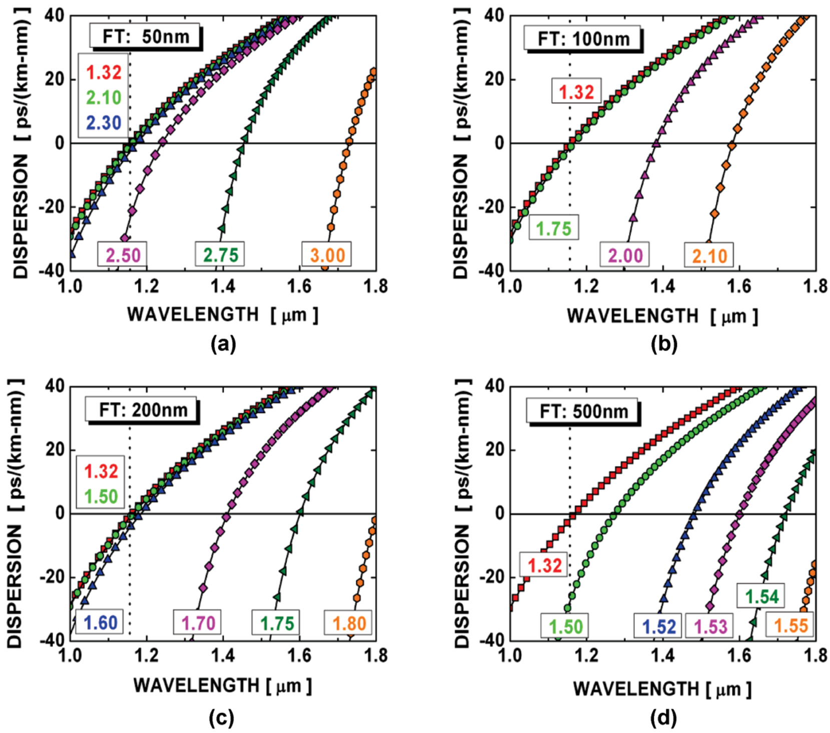

Figure 6. Dispersion as a function of the wavelength. The vertical dotted line shows the ZDW of the MOF without a film. Dispersion behaviors are: (a) for $FT = 50$ nm and $Nc = 1.32$, 2.10, 2.30, 2.50, 2.75, and 3.00; (b) for $FT = 100$ nm and $Nc = 1.32$, 1.75, 2.00, and 2.10; (c) for $FT = 200$ nm and $Nc = 1.32$, 1.50, 1.60, 1.70, 1.75, and 1.80; and (d) for $FT = 500$ nm and $Nc = 1.32$, 1.50, 1.52, 1.53, 1.54, and 1.55. (color figure available online)

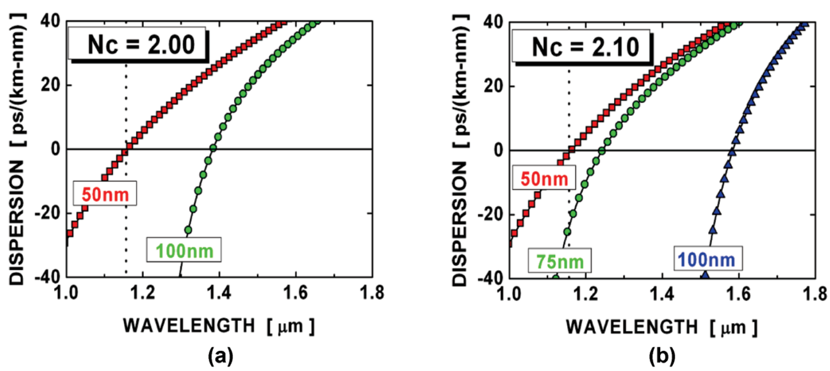

Figure 7. Dispersion as a function of the wavelength: (a) for $Nc = 2.00$ and $FT = 50$ and 100 nm and (b) for $Nc = 2.10$ and $FT = 50$, 75, and 100 nm. The vertical dotted line shows the ZDW of the MOF without a film. (color figure available online)

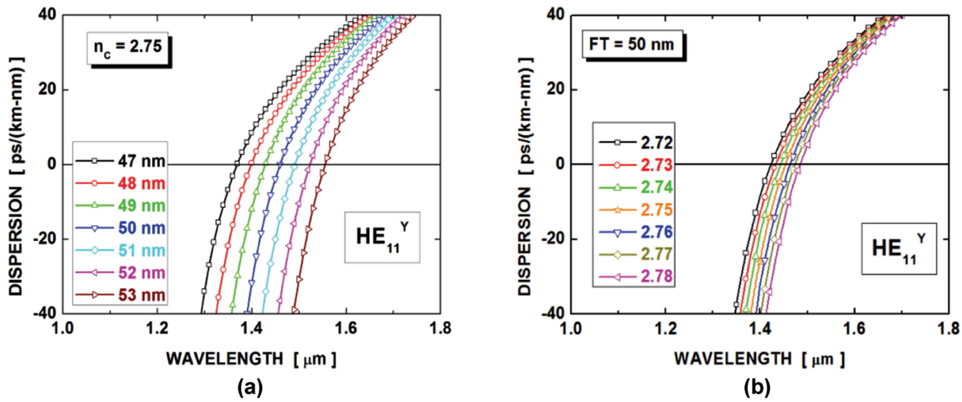

Figure 8. Sensitivity curves of the ZDW. Dispersion as a function of the wavelength: (a) for $Nc = 2.75$ and $FT = 47$, 48, 49, 50, 51, 52, and 53 nm and (b) for $FT = 50$ nm and $Nc = 2.72$, 2.73, 2.74, 2.75, 2.76, 2.77, and 2.78. (color figure available online)

Figure 8 shows the sensitivity curves for the ZDW with respect to the film thickness and index. Figure 8b, for $Nc = 2.75$, shows the sensitivity for diverse film thicknesses ranging from 47 nm to 53 nm; and a variation of the ZDW of 30 nm can be seen for each variation of 1 nm in the film thickness. Figure 8a, when $FT = 50$ nm, shows the sensitivity for diverse film indexes ranging from 2.72 to 2.78, where a variation of the ZDW of 10 nm can be observed for each variation of 0.01 in the refractive index of the film.

4. Conclusions

In this work, an effective way to control the zero dispersion of an MOF was proposed. The MOF is composed of a six-hole ring around the solid core and a thin film covering the inner surfaces of the holes.

The only parameters used to control the MOF dispersion were the thickness and the index of the film.

The numerical results in this study show that it is possible to control the MOF dispersion within a wavelength range from 1.0 to 1.8 μm.

The technique proposed here may be used to optimize the fiber dispersion control, and it may find important applications in telecommunication and non-linear optics.

References

1. Russell, P. 2003. Photonic crystal fibers. *Science* 299:358–362.
2. Knight, J. C. 2003. Photonic crystal fibres. *Nature* 424:847–851.
3. Sodré Jr, A. C. 2010. Recent progress and novel applications of photonic crystal fibers. *Report on Progress in Physics* 73:024401.
4. Saitoh, K., Koshiba, M., Hasegawa, T., and Sasaoka, E. 2003. Chromatic dispersion control in photonic crystal fibers: Application to ultra-flattened dispersion. *Optics Express* 11(8):843–852.
5. Shen, L. P., Huang, W. P. and Jian, S. S. 2003. Design of photonic crystal fibers for dispersion-related applications. *Journal of Lightwave Technology* 21(7):1644–1651.

6. Matsui, T., Zhou, J., Nakajima, K., and Sankawa, I. 2005. Dispersion-flattened photonic crystal fiber with large effective area and low confinement loss. *Journal of Lightwave Technology* 23(12): 4178–4183.
7. Saitoh, K., and Koshiba, M. 2005. Numerical modeling of photonic crystal fibers. *Journal of Lightwave Technology* 23(11):3580–3590.
8. Hernández-Figueroa, H. E., Fernández, F. A., Lu, Y., and Davies, J. B. 1995. A vectorial finite element formulation for analysing 2D leaky waveguides. *IEEE Transactions on Magnetics* 31(3):1710–1713.
9. da Silva, J. P., Hernández-Figueroa, H. E., and Frasson, A. M. F. 2003. Improved vectorial finite-element BPM analysis for transverse anisotropic media. *Journal of Lightwave Technology* 21(2):567–576.
10. da Silva, J. P., Bezerra, D. S., Rodríguez-Esquerre, V. F., da Fonseca, I. E., and Hernández-Figueroa, H. E. 2010. Ge-doped defect-core microstructured fiber design by genetic algorithm for residual dispersion compensation. *IEEE Photonics Technology Letters* 22(18):1337–1339.
11. Koshiba, M., and Inoue, K. 1992. Simple and efficient finite-element analysis of microwave and optical waveguides. *IEEE Transactions on Microwave Theory and Techniques* 40(2):371–377.
12. Brechet, F., Marcou, J., Pagnoux, D., and Roy, P. 2000. Complete analysis of the characteristics of propagation into photonic crystal fibers, by the finite element method. *Optical Fiber Technology* 6(2):181–191.
13. Guenneau, S., Nicolet, A., Zolla, F., and Lasquellec, S. 2002. Modeling of photonic crystal optical fibers with finite elements. *IEEE Transactions on Magnetics* 38(2):1261–1264.
14. Khedim, S., Chiali, A., Benyoucef, B., and Chabane Sari, N. E. 2007. Calculation of refractive index of some materials. *Revue des Energies Renouvelables (ICRESD-07)*, Tlemcen, Algeria, May 21–24, pp. 337–341.

Biographies

Roddy E. Ramos Gonzáles was born in Miraflores, Lima, Peru. He received his B.S. in physics from the School of Science–FC, National University of Engineering–UNI, Lima, Peru, in 1999, and his M.Sc. in physics from the Department of Quantum Electronics—DEQ, Gleb Wataghin Physics Institute–IFGW, University of Campinas–UNICAMP, Campinas, Brazil, in 2003. He is currently pursuing his Ph.D. in the Department of Microwaves and Optics–DMO, School of Electrical and Computer Engineering–FEEC, University of Campinas–UNICAMP, Campinas, Brazil. His research interests include computational electromagnetic waves, integrated optics, and nonlinear optics.

Enver Fernández Chillcce received this B.S. in physics from the School of Science–FC, National University of Engineering–UNI, Lima, Peru, in 1996, and his PhD in physics at the Department of Quantum Electronics–DEQ, Gleb Wataghin Physics Institute–IFGW, University of Campinas–UNICAMP, Campinas, Brazil, in 2005.

Luiz Carlos Barbosa was born in Limeira–SP Brazil, 1945. He received his Ph.D. in Physics from the University of Campinas, Campinas, Brazil, in 1981. His research field is photonic optical fibers, but recently he began to focus on glasses for optical devices. He has published around 100 papers in indexed journals and 200 papers in international congresses.

Hugo E. Hernández-Figueroa received his B.Sc. in electrical engineering from the Federal University of Rio Grande do Sul, Porto Alegre, Brazil, in 1983; his M.Sc. in electrical engineering and M.Sc in informatics, both from the Pontifical Catholic University of Rio de Janeiro, Rio de Janeiro, Brazil, in 1985 and 1987, respectively; and his Ph.D. in physics from the Imperial College of Science, Technology and Medicine, University of London, UK, in 1992. After spending two years as a postdoctoral fellow with the Department of Electronic and Electrical Engineering, University College London (UCL), London, UK, he joined the University of Campinas (UNICAMP), School of Electrical and Computer Engineering (FEEC), Department of Microwaves and Optics (DMO), as an assistant professor, in 1995. In 2005, he became a full professor, and since 2006 he has been head of the DMO. He has published over 80 papers in renowned journals and over 150 international conference papers. He is co-editor of the book *Localized Waves: Theory and Applications*. His research interests include a wide variety of wave electromagnetic phenomena and applications mainly in photonics and microwaves. He is also involved in research projects dealing with information technology applied to technology-based education. He has been very active with IEEE (Photonics Society, Microwave Theory and Techniques Society, and Education Society) and the Optical Society of America (OSA) for the last 16 years, acting as organizer for several international conferences, guest editor for special issues, an AdCom member, and a Chapter Chair. Since 2001, he has been a member of the editorial board of *IEEE Transactions on Microwave, Theory, and Techniques*; was an associate editor (Opto-Electronics/Integrated Optics) of *IEEE/OSA Journal of Lightwave Technology*; and was the general co-chair of the *OSA Integrated Photonics and Nanophotonics Research and Applications (IPNRA)* 2008 topical meeting. He received the IEEE Third Millennium Medal in 2000.